

Magnetars: Super(ficially) hot and super(fluid) cool

Wynn C. G. Ho,^{1*} Kostas Glampedakis,^{2,3} and Nils Andersson¹

¹*School of Mathematics, University of Southampton, Southampton, SO17 1BJ*

²*Departamento de Física, Universidad de Murcia, E-30100 Murcia, Spain*

³*Theoretical Astrophysics, University of Tübingen, Auf der Morgenstelle 10, Tübingen D-72076, Germany*

Accepted 2012 February 25. Received 2012 February 24; in original form 2011 November 30

ABSTRACT

We examine to what extent the inferred surface temperature of magnetars in quiescence can constrain the presence of a superfluid in the neutron star core and the role of magnetic field decay in the core. By performing detailed simulations of neutron star cooling, we show that extremely strong heating from field decay in the *core* cannot produce the high observed surface temperatures nor delay the onset of neutron superfluidity in the core. We verify the results of Kaminker et al., namely that the high magnetar surface temperatures require heating in the neutron star *crust*, and crust heating is decoupled from cooling/heating in the core. Therefore, because crust heating masks core heating, it is not possible to conclude that magnetar cores are in a non-superfluid state purely from high surface temperatures. From our interior temperature evolutions and after accounting for proton superconductivity in the core, we find that neutron superfluidity in the core occurs less than a few hundred years after neutron star formation. This onset time is unaffected by heating due to core field decay at fields $\lesssim 10^{16}$ G. Thus all known neutron stars, including magnetars, without a core containing exotic particles, should have a core of superfluid neutrons and superconducting protons.

Key words: dense matter — neutrinos — pulsars: general — stars: evolution — stars: magnetars — stars: neutron

1 INTRODUCTION

Neutron stars (NSs) begin their lives very hot (with temperatures $T > 10^{11}$ K) but cool rapidly through the emission of neutrinos. Neutrino emission processes depend on uncertain physics at the supra-nuclear densities ($\rho > \rho_{\text{nuc}} \approx 2.8 \times 10^{14}$ g cm⁻³) of the NS core (see Tsuruta 1998; Yakovlev & Pethick 2004; Page et al. 2006, for review). Current theories indicate that the core may contain a neutron superfluid and proton superconductor or even exotic particles, such as hyperons and deconfined quarks (see, e.g., Lattimer & Prakash 2004; Haensel et al. 2007, for review). The recent observation of rapid cooling (Heinke & Ho 2010; Shternin et al. 2011) of the NS in the Cassiopeia A supernova remnant provides the first constraints on the critical temperatures for the onset of superfluidity of core neutrons T_{cnt} (in the triplet state) and protons T_{cp} (in the singlet state), i.e., $T_{\text{cnt}} \approx (5 - 9) \times 10^8$ K and $T_{\text{cp}} \sim (2 - 3) \times 10^9$ K (Page et al. 2011; Shternin et al. 2011).

Anomalous X-ray pulsars and soft gamma-ray repeaters form the magnetar class of NSs, i.e., systems which pos-

sess superstrong magnetic fields ($B \gtrsim 10^{14}$ G)¹, and their strong fields likely power the activity seen in these objects (see Woods & Thompson 2006; Mereghetti 2008, for review). One notable property of magnetars is that their observed surface temperatures T_s in quiescence are significantly higher than those of other NSs of a similar age. In fact, they are too high for NSs that cool passively, i.e., without an additional source of internal heat (accretion heating can be excluded by, e.g., non-detections of binary companion or disk emission). An interesting problem concerns the heat generated from magnetic field decay, which has been proposed to be the source for the high temperatures of magnetars (Thompson & Duncan 1996; Heyl & Kulkarni 1998; Colpi et al. 2000; Aguilera et al. 2008b). This heat can strongly influence the time/age at which the core becomes superfluid if heating/field decay occurs in the core (Thompson & Duncan 1996; Arras et al. 2004; Dall’Osso et al. 2009). The problem is important since the presence of superfluid components has a strong impact on magnetar interior dynamics, such

* Email: wynnho@slac.stanford.edu

¹ However, there exists an apparently low surface magnetic field magnetar (Rea et al. 2010).

as the mechanism for producing glitches (see, e.g., Sauls 1989), fluid oscillations (see, e.g., Passamonti & Andersson 2011), magnetic field and rotational evolution (see, e.g., Glampedakis & Andersson 2011), and magnetohydrodynamical equilibrium (Glampedakis et al. 2012; Lander et al. 2012).

We address this problem by conducting detailed calculations of the thermal evolution of a NS with various prescriptions for an internal heat source that can be associated with magnetic field decay. We show that, regardless of the magnetic field strength and detailed mechanism for field decay in the core, the heat generated by the decay is insufficient to power the surface emission of magnetars. Furthermore, by accounting for the effects of proton superconductivity on field decay, we find that this core heating is not strong enough to balance neutrino cooling and cannot delay the onset of core neutron superfluidity for fields $\lesssim 10^{16}$ G (onset at age \lesssim a few $\times 100$ yr). Thus the cores of all currently known magnetars should be in a superfluid state.

We briefly describe past works and note key findings and assumptions made in these works that we improve upon here. Arras et al. (2004) consider coupled magnetic field decay and thermal evolution of magnetars. The internal field and superfluid temperatures are assumed to be $> 10^{15}$ G and $T_{\text{cp}} = 5 \times 10^9$ K and $T_{\text{cnt}} = (5 - 9) \times 10^8$ K, respectively. Arras et al. (2004) find that magnetic field decay can delay the transition to core neutron superfluidity and maintain a relatively high surface temperature to ages $\approx 10^3 - 10^5$ yr, depending on T_{cnt} . However, their calculation only considers volume-averaged quantities and thus assumes that the NS interior is isothermal (see Section 2.2), which cannot be the case if there is a localized heating source such as field decay in the crust or core due to the large but finite thermal conductivity of NS matter.

Kaminker et al. (2006) calculate the evolution of the temperature profile [i.e., $T(\rho)$] by solving the energy balance and flux equations [see eqs. (2) and (3)]. They demonstrate that, in order to explain the observed high surface temperatures, magnetars require a heat source and, most importantly, this heat source (e.g., from field decay; Pons et al. 2009) must be located in the outer crust; if the heat source is located too deep in the NS interior (e.g., in the core), then neutrino emission efficiently removes the heat locally, and the surface temperature cannot be increased sufficiently to match the observed values. Furthermore, the outer crust is thermally decoupled from the core so that heating of the crust does not affect (neutrino) cooling of the core. Because of this thermal decoupling, the results and conclusions of Kaminker et al. (2006) are not particularly sensitive to the state of matter in the core, e.g., superfluidity of the core nucleons. Though no quantitative results are shown, Kaminker et al. (2006) state that cooling calculations with the effects of inner crust superfluidity and neutrino emission by Cooper pair formation produce different temperature profiles, but these effects do not change the surface temperature. In follow-up work, Kaminker et al. (2009) improve their calculations and examine the effects of light-element accreted envelopes and anisotropic heat conduction due to the magnetic field in the envelope and outer crust. While accreted envelopes can give higher surface temperatures for the same core temperatures, core heating is still unable to

produce surface temperatures that are high enough to explain magnetar observations.

Dall’Osso et al. (2009) criticize the work of Kaminker et al. (2006), arguing that the phenomenological heating model considered is independent of magnetic field and decays on the wrong timescale [see eq. (16)] and that the correct heating should depend inversely on temperature. This last point implies that more heat is generated at lower temperatures and can lead to an equilibrium between neutrino cooling and heating from field decay (see also Thompson & Duncan 1996). The equilibrium temperature (above 10^9 K) can be maintained for $\approx 10^4$ yr. The results of Dall’Osso et al. (2009) suggest that the core of magnetars are not superfluid until after this time, since the critical temperature for the onset of neutron superfluidity is $(5 - 9) \times 10^8$ K (Page et al. 2011; Shternin et al. 2011). However no cooling calculation is performed by Dall’Osso et al. (2009).

Here we perform NS cooling simulations to determine the role of core heating by magnetic field decay. We do not examine in detail field evolution and heating in the crust (see, e.g., Pons et al. 2009). Rather we use the phenomenological model of Kaminker et al. (2006, 2009) to demonstrate the effect of *crust heating* on the NS cooling behavior. This will be adequate for our purposes since the goal here is to assess the importance of *core heating* in magnetars. As we will show, as long as the magnetic field decay time is longer than the cooling time, the core heating we use is the maximum one can use. While this maximal heating can delay the onset of neutron superfluidity [on the timescale estimated by Thompson & Duncan (1996); Dall’Osso et al. (2009)], it cannot reproduce the high surface temperatures seen for magnetars. We arrive at this same conclusion using the prescription for heating and field decay given in Dall’Osso et al. (2009). Furthermore, the above works neglect the effects of proton superconductivity; when this is taken into account, there is no delay in superfluidity onset for any reasonable core magnetic field strength. In Section 2, we describe the thermal evolution equations and input physics, including superfluid properties and prescriptions for internal heat sources. Section 3 presents the results of our calculations. We summarize our results and discuss their implications in Section 4.

2 NEUTRON STAR COOLING MODEL

2.1 Core and Crust Composition

We use a stellar model based on the Akmal-Pandharipande-Ravenhall (APR) equation of state (EOS) (Akmal et al. 1998; Heiselberg & Hjorth-Jensen 1999), specifically APR I² (Gusakov et al. 2005). For a NS mass $M = 1.4 M_{\odot}$, the NS radius is $R = 12.1$ km, and the central density is $\rho_c = 9.47 \times 10^{14}$ g cm⁻³. The crust composition³ (in par-

² The maximum NS mass for this EOS is $1.923 M_{\odot}$, which is below the highest measured mass of $1.97 M_{\odot}$ (Demorest et al. 2010). Nevertheless, APR is typical of EOSs that yield higher maximum masses, and our conclusions do not depend strongly on the specific EOS.

³ See <http://relativity.livingreviews.org/Articles/lrr-2008-10/>

ticular, charge number Z and mass number A of the ions) as a function of density ρ is determined by interpolating the values taken from Table VII of R  ster et al. (2006) for $8.02 \times 10^6 \text{ g cm}^{-3} \leq \rho \leq 4.27 \times 10^{11} \text{ g cm}^{-3}$ and Table 3 of Negele & Vautherin (1973) for $4.67 \times 10^{11} \text{ g cm}^{-3} \leq \rho \leq 7.94 \times 10^{13} \text{ g cm}^{-3}$ and estimated from Figs. 6 and 9 of Oyamatsu (1993) for $\rho = (1, 1.5) \times 10^{14} \text{ g cm}^{-3}$. We note that the melting temperature T_{melt} is given by (see, e.g., Shapiro & Teukolsky 1983)

$$T_{\text{melt}} = 3.04 \times 10^7 \text{ K } (Z/26)^{5/3} (170/\Gamma_m)x, \quad (1)$$

where $x = [(Z/A)(\rho/10^6 \text{ g cm}^{-3})]^{1/3}$ and $\Gamma_m \approx 170$ is the value of the Coulomb parameter $\Gamma_c [= Z^2 e^2 / akT]$, where $a = (3/4\pi n_i)^{1/3}$ and n_i is the ion number density] at which melting occurs.

2.2 Equations for Neutron Star Cooling

The evolution of the interior temperature $T(r, t)$ of an isolated NS is determined by the relativistic equations of energy balance and heat flux, i.e.,

$$\frac{e^{-\Lambda-2\Phi}}{4\pi r^2} \frac{\partial}{\partial r} (e^{2\Phi} L_r) = -e^{-\Phi} C \frac{\partial T}{\partial t} - \varepsilon_\nu + Q_h \quad (2)$$

$$\frac{L_r}{4\pi r^2} = -e^{-\Lambda-\Phi} K \frac{\partial}{\partial r} (e^\Phi T), \quad (3)$$

where L_r is the luminosity at radius r , C is the heat capacity, ε_ν is the neutrino emissivity, Q_h is the internal heating source, and K is the thermal conductivity (see, e.g., Thorne 1977; Shapiro & Teukolsky 1983). The metric function Λ is defined by the enclosed mass $m(r)$, i.e., $e^{\Lambda(r)} \equiv [1 - 2Gm(r)/c^2 r]^{-1/2}$, $\Phi(r)$ is the metric function (gravitational potential in Newtonian limit) that is obtained from $d\Phi/dr = -(dP/dr)/[\rho(1 + P/\rho)]$, and $e^{-\Lambda(R)} = e^{\Phi(R)}$ at the NS surface. We define (see, e.g., van Riper 1991)

$$\tilde{T} \equiv e^\Phi T \quad \text{and} \quad \tilde{L} \equiv e^{2\Phi} L_r, \quad (4)$$

so that eqs. (2) and (3) become

$$\frac{\partial \tilde{L}}{\partial r} = -4\pi r^2 e^\Lambda C \frac{\partial \tilde{T}}{\partial t} - 4\pi r^2 e^{\Lambda+2\Phi} (\varepsilon_\nu - Q_h) \quad (5)$$

$$\tilde{L} = -4\pi r^2 K e^{-\Lambda+\Phi} \frac{\partial \tilde{T}}{\partial r}, \quad (6)$$

respectively. Thus the inputs that determine how a NS cools are the heat capacity C , neutrino emissivity ε_ν , thermal conductivity K , and heat source Q_h . The following sections discuss the physics that determine the four physical parameters, C , ε_ν , K , and Q_h . We note that, due to the high thermal conductivity, NSs without additional heat sources ($Q_h = 0$) become essentially isothermal after $\sim 10 - 100 \text{ yr}$ (Lattimer et al. 1994; Gnedin et al. 2001; Yakovlev et al. 2011). When isothermal, the thermal evolution is determined solely by eq. (5), which can be simplified by integrating over the volume. The evolution of the interior temperature is solved by a method similar to that described in Gnedin et al. (2001) (see also Yakovlev & Pethick 2004; Page et al. 2006, for review).

Table 1. Phenomenological parameters for superfluid gap energy

	proton singlet	neutron singlet	shallow neutron triplet	deep neutron triplet
Δ_0 (MeV)	120	68	0.068	0.15
k_0 (fm $^{-1}$)	0	0.1	1.28	2
k_1 (fm $^{-2}$)	9	4	0.1	0.1
k_2 (fm $^{-1}$)	1.3	1.7	2.37	3.1
k_3 (fm $^{-2}$)	1.8	4	0.02	0.02

2.3 Superfluid Properties

Superfluidity has two important effects on neutrino emission and NS cooling: (1) suppression of heat capacities and emission mechanisms, like modified Urca processes, that involve superfluid constituents and (2) enhanced emission due to Cooper pairing of nucleons when the temperature decreases just below the critical value (see Yakovlev & Pethick 2004; Page et al. 2006, for review).

The critical temperatures for superfluidity are approximately related to the superfluid energy gap Δ by $kT_c \approx 0.5669\Delta$ for the singlet (isotropic pairing) gap and $kT_c \approx 0.8418\Delta$ for the maximum triplet (anisotropic pairing) gap. We use the parametrization for the gap energy

$$\Delta(k_{\text{Fx}}) = \Delta_0 \frac{(k_{\text{Fx}} - k_0)^2}{(k_{\text{Fx}} - k_0)^2 + k_1} \frac{(k_{\text{Fx}} - k_2)^2}{(k_{\text{Fx}} - k_2)^2 + k_3}, \quad (7)$$

where $p_{\text{Fx}} = \hbar k_{\text{Fx}} = \hbar(3\pi^2 n_x)^{1/3}$ and n_x are the Fermi momentum and number density, respectively, for particle x and Δ_0 , k_0 , k_1 , k_2 , and k_3 are fit parameters for particular superfluid gap models given in Andersson et al. (2005) (see also Lombardo & Schulze 2001; Kaminker et al. 2002). For singlet neutrons in the crust, we use model *a*, which represents the results of Wambach et al. (1993). For singlet protons in the core, we use a model that is similar to Chen et al. (1993) (see also Page et al. 2004). We consider two cases for triplet neutron pairing in the core. Either the pairing is the “shallow” model *l*, which represents the results of Elgar  y et al. (1996), or the pairing is a “deep” model. The deep model is a Δ that produces a $T_{\text{cnt}}(\rho)$ similar to what is needed to fit the observed surface temperature of the neutron star in Cassiopeia A and neutron stars that are old and hot (Gusakov et al. 2004, 2005; Shternin et al. 2011). The parameters for the superfluid gap energies are given in Table 1, and the gap models are illustrated in Figs. 1 and 2.

2.4 Heat Capacity

In the core, the total heat capacity is the sum of partial heat capacities due to neutrons, protons, electrons, and muons. In the crust, the total heat capacity is the sum of partial heat capacities due to free neutrons, ions, and electrons. The partial heat capacity for a strongly degenerate fermion particle species x is

$$C_x = \frac{m_x^* p_{\text{Fx}} k^2 T}{3\hbar^3}, \quad (8)$$

where m_x^* is the effective mass. We assume $m_x^* = 0.7$ for neutrons and protons and take $m_x^* = (m_x^2 c^4 + p_{\text{Fx}}^2 c^2)^{1/2}$ for

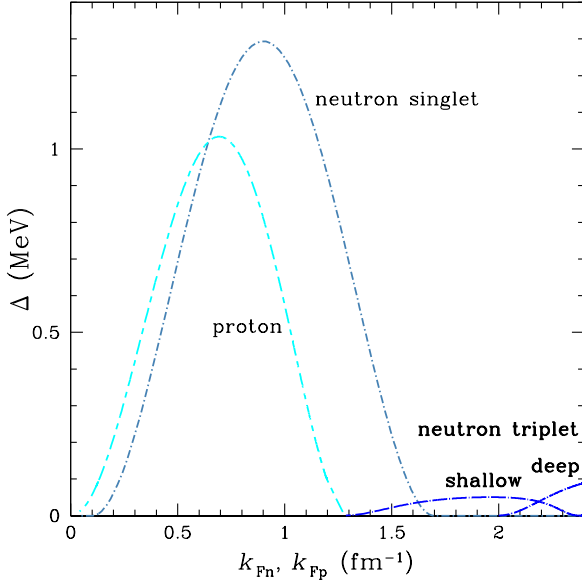


Figure 1. Superfluid gap energies (left: singlet; right: triplet) as a function of Fermi wavenumber for neutrons k_{Fn} and protons k_{Fp} . The neutron singlet (dot-short-dashed) model is from Wambach et al. (1993), the proton singlet (dashed) model is similar to Chen et al. (1993), and the neutron triplet (dot-long-dashed) model is either a shallow model from Elgarøy et al. (1996) or a deep model similar to Shternin et al. (2011).

electrons and muons. A reduction of the heat capacity due to nucleon superfluidity can be taken into account by using

$$C_x^{\text{SF}} = R_x^C C_x^C \quad (9)$$

where the reduction factor R_x^C only depends on the ratio T/T_{cx} and whether the superfluid is of singlet or triplet type (Levenfish & Yakovlev 1994a; Yakovlev et al. 1999b). The ion heat capacity is (van Riper 1991)

$$C_{\text{ion}} = (3/2)k \times \begin{cases} 1 & \text{if } \Gamma_c \leq 1 \\ 2f_D(T/T_D) & \text{if } 1 < \Gamma_c \leq 150 \\ 1 + \frac{\log \Gamma_c}{\log 150} & \text{if } \Gamma_c > 150 \end{cases}, \quad (10)$$

where

$$f_D(T/T_D) = \begin{cases} 0.8\pi^4(T/T_D)^3 & \text{if } T/T_D \leq 0.15 \\ 1 - 0.05(T_D/T)^2 & \text{if } T/T_D \geq 4 \\ 1.70(T/T_D) + 0.0083 & \text{otherwise} \end{cases} \quad (11)$$

and the Debye temperature is

$$T_D = 3.48 \times 10^6 \text{ K } (Z/A)(\rho/10^6 \text{ g cm}^{-3})^{1/2}. \quad (12)$$

2.5 Neutrino Emissivity

For the NS core, we calculate neutrino emission due to the neutron and proton branches of the modified Urca process and neutron-neutron, neutron-proton, and proton-proton bremsstrahlung using emissivities from Yakovlev et al. (1999b); Page et al. (2004). When neutrons and/or protons are superfluid, we account for suppression of the above processes (Levenfish & Yakovlev 1994b; Yakovlev et al. 1999b) and neutrino emission due to Cooper pairing of the superfluid component (Yakovlev et al. 1999b; Page et al. 2009).

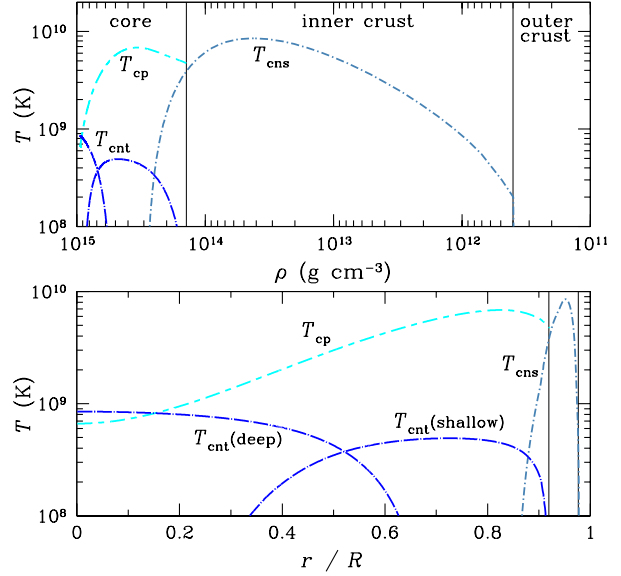


Figure 2. Superfluid critical temperatures as a function of density (top panel) and normalized stellar radius (bottom panel). Critical temperatures T_{cns} (dot-short-dashed), T_{cnt} (dot-long-dashed), and T_{cp} (dashed) are for neutron singlet, neutron triplet, and proton singlet, respectively. Neutron triplet pairing is taken to be described by either the shallow or deep model (see text). Vertical solid lines indicate the approximate boundaries between the core and inner crust (at near nuclear saturation, i.e., $\rho \approx \rho_{\text{nuc}}/2$) and inner and outer crusts (at neutron drip, i.e., $\rho \approx 4 \times 10^{11} \text{ g cm}^{-3}$).

For the APR I EOS (see Section 2.1), neutrino emission by the direct Urca process occurs when $M > 1.829 M_{\odot}$ (central densities above $1.680 \times 10^{15} \text{ g cm}^{-3}$; Gusakov et al. 2005); for this present work in which we consider only $M = 1.4 M_{\odot}$, we will neglect this process (as well as other ‘fast’ cooling processes; see Yakovlev & Pethick 2004; Page et al. 2006). As shown by Kaminker et al. (2006), cooling by direct Urca has no effect on the surface temperature because of thermal decoupling between the core and outer crust. In addition, since direct Urca is more effective at cooling the core, it would speed up the onset of superfluidity. Hence its inclusion would make our conclusions even more robust.

In the crust, we account for electron-nucleon, neutron-neutron, and neutron-nucleon bremsstrahlung, plasmon decay, and e^-e^+ pair annihilation using emissivities from Yakovlev et al. (1999a, 2001). When neutrons are superfluid (in the singlet state), we account for the suppression of neutron-neutron and neutron-nucleon bremsstrahlung (Yakovlev et al. 1999b, 2001), as well as including neutrino emission due to neutron Cooper pairing (Yakovlev et al. 1999b; Page et al. 2009). We neglect neutrino synchrotron emission in a magnetic field since this additional emission would cause even more rapid cooling of the crust (Yakovlev et al. 2001).

2.6 Thermal Conductivity

For the core, we sum thermal conductivities due to neutrons, electrons, and muons (Flowers & Itoh 1979, 1981). We use

the results of Baiko et al. (2001) to calculate the neutron thermal conductivity, accounting for neutron-neutron and neutron-proton collisions and superfluid suppression. We use the results of Shternin & Yakovlev (2007) to calculate the electron and muon thermal conductivities and account for superfluid suppression. For the crust, we use CONDUCT08⁴, which implements the latest advancements in calculating thermal conductivities (Potekhin et al. 1999; Cassisi et al. 2007; Chugunov & Haensel 2007). We assume no contribution by impurity scattering, which only becomes important at high densities and low temperatures.

At high magnetic fields and low temperatures, electron motion is strongly influenced by the magnetic field (see, e.g., Yakovlev & Kaminker 1994). As a result, the electrical and thermal conductivities become anisotropic, depending on whether electrons move parallel or transverse to the direction of the field (Potekhin 1999). However, electron magnetization and anisotropic heat conduction are weaker at higher temperatures (see Lai 2001, for review). In particular, magnetic field effects are minimal when the field is in the non- or weakly-quantizing regime, i.e., when $T > T_B$ and $\rho \gg \rho_B$, where

$$T_B = 1.34 \times 10^{10} \text{ K } (B/10^{14} \text{ G})(1+x^2)^{-1/2}, \quad (13)$$

x is defined below eq. (1), and $\rho_B = 7.046 \times 10^6 \text{ g cm}^{-3} (A/Z)(B/10^{14} \text{ G})^{3/2}$. Since we are primarily concerned with effects in the high density core of young NSs with high interior temperatures and the core is effectively thermally decoupled from the crust (Kaminker et al. 2006, 2009), we neglect magnetic field effects on the conductivities below the heat blanket (see also Section 2.7). In fact, recent works show that the effects of superfluid phonons (Aguilera et al. 2009) and toroidal magnetic fields (Pons et al. 2009) in the crust can very effectively smooth out temperature variations induced by anisotropic heat conduction.

2.7 Envelope

The outer layers (envelope) of the NS crust serve as a heat blanket, and there can exist a large temperature gradient between the bottom of the envelope (at ρ_{env} and T_{env}) and the surface. We assume $\rho_{\text{env}} = 10^{10} \text{ g cm}^{-3}$ (see, e.g., Gudmundsson et al. 1982; Yakovlev & Pethick 2004). Chang & Bildsten (2004) (see also Chang et al. 2010) show that, at the high temperatures present in magnetars, nuclear burning very rapidly removes any surface hydrogen; nevertheless, for generality, we consider surfaces composed of either iron or light-elements. For iron, the relationship between the temperature at the bottom of the heat-blanketing envelope T_{env} and the effective temperature of the photosphere T_s is (Gudmundsson et al. 1982)

$$T_s = 8.7 \times 10^5 \text{ K } g_{s,14}^{1/4} (T_{\text{env}}/10^8 \text{ K})^{11/20}, \quad (14)$$

where $g_{s,14} = g_s/10^{14} \text{ cm s}^{-2}$ and $g_s = (1 - 2GM/c^2 R)^{-1/2} GM/R^2$ is the surface gravity ($g_{s,14} = 1.55$ for our assumed NS model). Non-magnetized envelopes composed of light elements (H or He) have been considered in

Potekhin et al. (1997) [Kaminker et al. (2009) find a negligible difference in the results using either H or He at $T_{\text{env}} > 10^8 \text{ K}$; see also Yakovlev et al. 2011, for carbon envelopes]. Due to the higher thermal conductivity ($\propto Z^{-1}$) of light elements, the difference between T_s and T_{env} is larger for a light-element envelope compared to an iron envelope, i.e., T_s is higher for a given T_{env} and T_{env} is lower for a given T_s . For a fully-accreted light element envelope (Potekhin et al. 1997),

$$T_s = 1.43 \times 10^6 \text{ K } g_{s,14}^{1/4} (T_{\text{env}}/10^8 \text{ K})^{17/28}. \quad (15)$$

For clarity, we show the above relations [eqs. (14) and (15)]; however, we use the more accurate expressions given in Potekhin et al. (2003) in our calculations.

Magnetized envelopes produce higher (lower) T_s for a given T_{env} due to enhanced (reduced) thermal conduction along (across) the magnetic field, and the effect is stronger for accreted envelopes (Potekhin & Yakovlev 2001; Potekhin et al. 2003). Kaminker et al. (2006, 2009) include the effects of magnetic fields ($\sim 10^{14} - 10^{16} \text{ G}$) in the envelope and inner and outer crusts and find that, though the temperature profile in the crust is modified, the average surface temperature is only weakly affected by anisotropic heat conduction. We mostly neglect magnetized envelopes since their effects would not significantly affect our conclusions (see Section 3.5).

2.8 Heat Source

We consider several prescriptions for an internal heat source. For heating in the crust, we use a model similar to the phenomenological one of Kaminker et al. (2006, 2009), i.e.,

$$Q_h = Q_0 \exp\{-(\rho - \rho_h)/\Delta_h\}^2 \exp(-t/\tau_h); \quad (16)$$

the exact form of heating is unimportant, as demonstrated by Kaminker et al. (2009). We take $\tau_h = 10^4 \text{ yr}$, $Q_0 = 3 \times 10^{20} \text{ ergs cm}^{-3} \text{ s}^{-1}$, $\rho_h = 6 \times 10^{10} \text{ g cm}^{-3}$, and $\Delta_h = 2 \times 10^{10} \text{ g cm}^{-3}$. The total heat luminosity $L_h = \int Q_h e^{2\Phi} 4\pi r^2 dr \approx 10^{37} \text{ ergs s}^{-1}$ at $t \ll \tau_h$. Note that Kaminker et al. (2006, 2009) use a heating decay timescale $\tau_h = 5 \times 10^4 \text{ yr}$; the exact value is unimportant for our purposes, as long as it is approximately the age of the oldest (high surface temperature) magnetar, since τ_h is approximately the time during which a high surface temperature can be maintained by this crust heating (see Section 3.5).

In the core, heating is supplied by magnetic field decay due to ambipolar diffusion (Goldreich & Reisenegger 1992). We estimate a heating rate

$$Q_h \approx \frac{B}{4\pi} \frac{dB}{dt} \approx \frac{B^2}{4\pi\tau^{\text{amb}}} = 1 \times 10^{20} \text{ ergs cm}^{-3} \text{ s}^{-1} \times \left(\frac{\rho}{\rho_{\text{nuc}}}\right)^{-2/3} \left(\frac{T}{10^9 \text{ K}}\right)^{-2} \left(\frac{B}{10^{16} \text{ G}}\right)^4, \quad (17)$$

where the ambipolar diffusion timescale τ^{amb} is given by (Goldreich & Reisenegger 1992)

$$\tau^{\text{amb}} \sim 2.5 \times 10^3 \text{ yr } (L/1 \text{ km})^2 (\rho/\rho_{\text{nuc}})^{2/3} \times (T/10^9 \text{ K})^2 (B/10^{16} \text{ G})^{-2} \quad (18)$$

and we neglect here the proton fraction dependence and assume the field decay lengthscale L ($= 1 \text{ km}$) is constant for simplicity. Heating is taken to occur throughout the core and

⁴ <http://www.ioffe.ru/astro/conduct/>

is thus very strong. Note that eq. (17) is identical to what is considered by Dall’Osso et al. (2009), except for a small difference in the numerical coefficient. It is also worth noting that τ^{amb} is the timescale of the “solenoidal” mode. This mode is controlled by collisions between the different particle species in NS matter and operates at relatively high temperatures (\gtrsim a few $\times 10^8$ K). Superfluidity can significantly modify τ^{amb} and thus the heating rate given by eq. (17). This is discussed in more detail in Section 3.6.

It is not well-understood how magnetic field decays (if at all) in the core at times $t \lesssim 10^4$ yr (see, e.g., Haensel et al. 1990; Goldreich & Reisenegger 1992; Thompson & Duncan 1996; Glampedakis et al. 2011). Therefore, to describe the decay of the core magnetic field, we use the simple formula

$$B(t) = \frac{B_0}{1 + t/\tau_{\text{decay}}}, \quad (19)$$

where τ_{decay} is the field decay timescale, which we choose to be 10^4 yr. Though eq. (19) has no physical basis, it has a form similar to ones considered in the literature, usually with the denominator (i.e., time-dependence) to some low-order power (see, e.g., Thompson & Duncan 1996; Colpi et al. 2000; Dall’Osso et al. 2009).⁵ However, recall that our aim is to obtain a *maximum* core heating rate, in order to test the extent to which core heating can produce the observed (high) surface temperature of magnetars and delay the onset of superfluidity. It is clear that eq. (17) is maximal before significant field decay, i.e., $B = B_0$ at $t \ll \tau_{\text{decay}}$. [At $t = 10^3$ yr, we find $L_h \sim 2 \times 10^{38}$ ergs s $^{-1}$ ($B/10^{16}$ G) 4 .] Therefore, as long as τ_{decay} is longer than the thermal diffusion timescale, this core heating will have a maximum effect on the surface temperature. We also conduct simulations utilizing the heating rate and field decay formulae from Dall’Osso et al. (2009) and find very similar results at the ages of interest here ($< 10^5$ yr).

3 RESULTS

We assume a constant $Te^\Phi = 10^{10}$ K at $t = 0$. For clarity, the superfluid results shown in all subsequent figures use the shallow neutron triplet model (see Section 2.3); the superfluid results using the deep neutron triplet model are qualitatively similar in the age range considered here ($< 10^5$ yr). Also we assume an iron envelope, unless noted otherwise. For models which include core heating, we primarily assume an initial magnetic field $B_0 = 10^{16}$ G, though we also consider lower, more realistic initial field strengths, as well as extreme fields.

⁵ Thompson & Duncan (1996) has a 1/14-th power of the denominator and a decay timescale proportional to τ^{amb} , while Dall’Osso et al. (2009) has a 5/6-th power of the denominator and a decay timescale given by 1.03×10^4 yr $(B/10^{16}$ G) $^{-6/5} (\rho/10^{15}$ g cm $^{-3}$) $^{2/5}$. The different evolution laws reflect the different ambipolar diffusion modes (solenoidal vs non-solenoidal) considered by these authors. Note that these decay timescales are shorter for higher magnetic fields. Incidentally, numerical simulations of field evolution in the crust yield eq. (19), with τ_{decay} given by the timescale for Hall drift at times much shorter than the Ohmic decay timescale (Aguilera et al. 2008a,b).

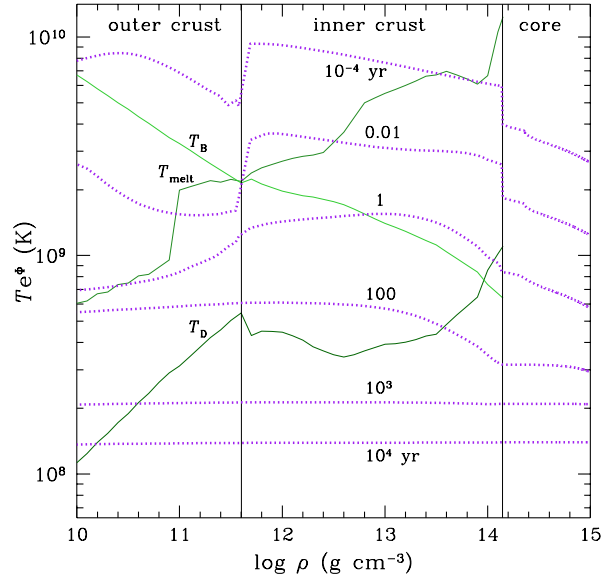


Figure 3. Temperature profiles for cooling model with no superfluidity and no heating (dotted lines). The six profiles are at ages $t = 10^{-4}$ (top), 0.01, 1, 100, 10^3 , and 10^4 yr (bottom). Thin solid lines denote the melting temperature T_{melt} , Debye temperature T_D , and T_B , where T_B is calculated assuming $B = 10^{15}$ G [see eq. (13)]. Vertical solid lines indicate boundaries between core and inner crust and inner and outer crusts.

3.1 Cooling with no superfluid nor heating

Figure 3 shows the temperature as a function of density at different ages for a NS cooling model that neglects superfluidity and has no additional sources of internal heating ($Q_h = 0$). These temperature profiles are very similar to those shown in Gnedin et al. (2001). At very early times, the core cools more rapidly than the crust via stronger neutrino emission, so that the crust is generally at higher temperatures. A cooling wave travels from the core to the surface, bringing the NS to a relaxed, isothermal state. Depending on the properties of the crust, the relaxation time is $\sim 10 - 100$ yr (Lattimer et al. 1994; Gnedin et al. 2001; Yakovlev et al. 2011). Formation of the inner and outer crusts begins at ~ 1 hr and ~ 1 day, respectively, and is mostly complete after ~ 1 month and ~ 1 yr, respectively (see also Aguilera et al. 2008a). The temperature profiles demonstrate the need to account for magnetic field effects in more accurate models of the crust and envelope when $T \lesssim T_B$ and temperature gradients are significant (see Sections 2.6 and 2.7).

3.2 Cooling with np superfluid and no heating

Figure 4 shows $T(\rho)$ at different ages for a cooling model that neglects heating but includes superfluidity of neutrons and protons, with critical temperatures also shown. When superfluidity is taken into account, we see the impact of the two effects mentioned in Section 2.3: Slower cooling in the core after protons become superconducting and faster cooling after neutrons become superfluid due to neutrino emission from Cooper pair formation. The latter is strongest

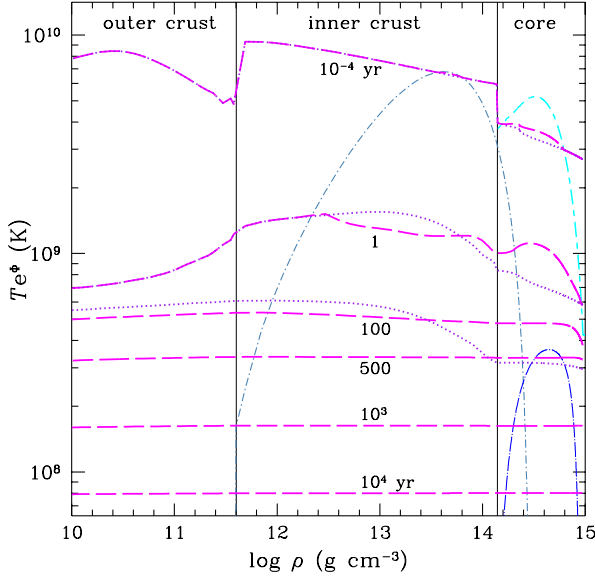


Figure 4. Temperature profiles for cooling model with superfluidity and no heating (long-dashed lines). The six profiles are at ages $t = 10^{-4}$ (top), 1, 100, 500, 10^3 , and 10^4 yr (bottom). Also plotted for comparison are profiles (dotted lines) for the model with no superfluidity at ages $t = 10^{-4}$, 1, and 100 yr (see Fig. 3). Critical temperatures for neutron singlet (dot-short-dashed), neutron triplet (dot-long-dashed), and proton singlet (short-long-dashed) are shown. Vertical solid lines indicate boundaries between core and inner crust and inner and outer crusts.

in regions near the critical temperature. Proton superconductivity occurs at ~ 1 min, and much of the core is superconducting after ~ 1 yr. Core neutrons start becoming superfluid at around a few $\times 100$ yr.

3.3 Cooling with superfluid and crust heating

Figure 5 shows temperature profiles for a cooling model that includes superfluidity and crust heating [see eq. (16)]. The profiles with crust heating are similar to those shown in Kaminker et al. (2006, 2009). In particular, it is clear that an additional heat source in the outer crust can very effectively maintain a high temperature near the NS surface [with redshifted surface temperature $T_s^\infty > 3 \times 10^6$ K, where $T_s^\infty = T_s(1 - 2GM/c^2R)^{1/2}$, for times longer than $\tau_h (= 10^4$ yr)], but this strong heating in the crust does not prevent the core from cooling rapidly. Due to thermal decoupling between the outer crust and core, the core temperature drops below the critical temperature for neutron triplet superfluidity at a few $\times 100$ yr, whether or not there is crust heating.

3.4 Cooling with superfluid and normal core heating

Figure 6 shows temperature profiles for a model that includes superfluidity and core heating due to magnetic field decay with an initial field $B_0 = 10^{16}$ G and $\tau_{\text{decay}} = 10^4$ yr [see eqs. (17) and (19)]. We see that, with such strong heating, the core temperature stays above the critical temper-

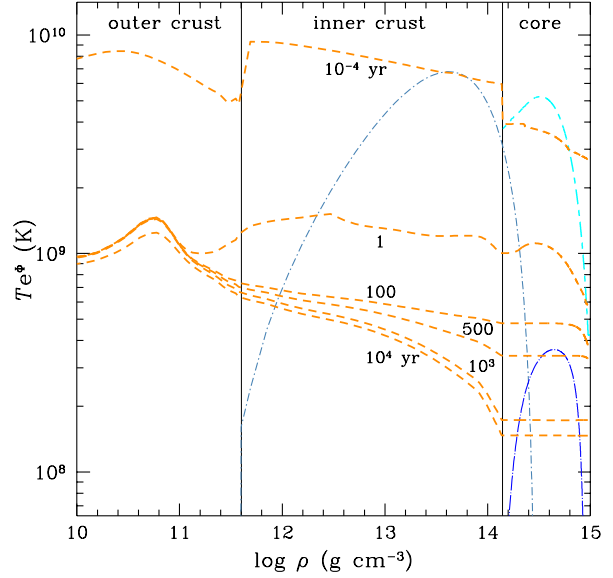


Figure 5. Temperature profiles for cooling model with superfluidity, crust heating, and heating timescale $\tau_h = 10^4$ yr (short-dashed lines). The six profiles are at ages $t = 10^{-4}$ (top), 1, 100, 500, 10^3 , and 10^4 yr (bottom). Critical temperatures for neutron singlet (dot-short-dashed), neutron triplet (dot-long-dashed), and proton singlet (short-long-dashed) are shown. Vertical solid lines indicate boundaries between core and inner crust and inner and outer crusts.

ature T_{cnt} for $t \gg 100$ yr. However, the extra heat created in the core from field decay is efficiently removed by core neutrino emission processes, with their strong temperature dependencies (Yakovlev & Pethick 2004; Page et al. 2006); while the temperatures in the crust are higher than those from models without any heating, they are significantly lower than those from models with crust heating.

3.5 Comparison with magnetar surface temperatures

Figure 7 shows the evolution of redshifted surface temperatures T_s^∞ for the cooling models plotted in Figs. 3 – 6. For models with crust or core heating, we also show cooling curves with fully accreted light element envelopes and a surface magnetic field 10^{15} G that is directed along the radial direction, which produce higher surface temperatures for the same outer crust temperature (Potekhin et al. 2003; see also Section 2.7). The cooling curves are compared to the estimated ages and measured surface temperatures of magnetars⁶ and other neutron stars (see Chevalier 2005; Yakovlev et al. 2008; Ho & Heinke 2009; Kaminker et al. 2009, and references therein). Our results clearly indicate

⁶ Data are taken from the McGill SGR/AXP Online Catalog at <http://www.physics.mcgill.ca/~pulsar/magnetar/main.html>. Magnetar ages and surface temperatures are not well-determined due to additional systematic uncertainties that are large (see, e.g., Kaminker et al. 2006, 2009, for details). Kaminker et al. (2009) consider the more reliable surface luminosity. For simplicity, we consider the “magnetar box” illustrated in Fig. 7.

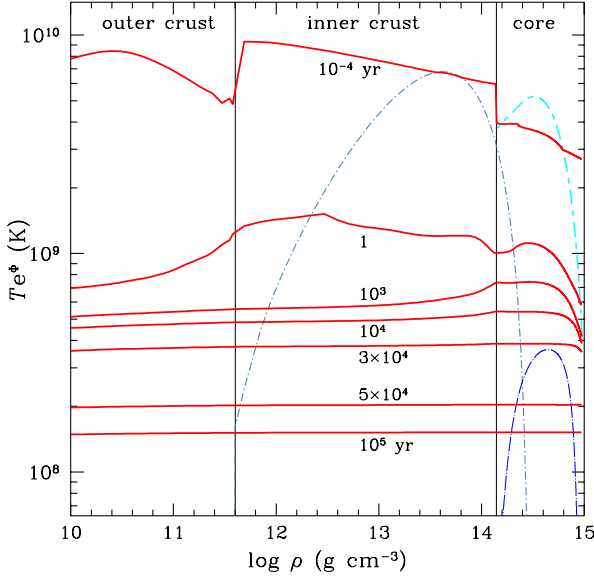


Figure 6. Temperature profiles for cooling model with superfluidity, normal core heating, initial magnetic field $B_0 = 10^{16}$ G, and field decay timescale $\tau_{\text{decay}} = 10^4$ yr (solid lines). The seven profiles are at ages $t = 10^{-4}$ (top), 1, 10^3 , 10^4 yr, 3×10^4 , 5×10^4 , and 10^5 yr (bottom). Critical temperatures for neutron singlet (dot-short-dashed), neutron triplet (dot-long-dashed), and proton singlet (short-long-dashed) are shown. Vertical solid lines indicate boundaries between core and inner crust and inner and outer crusts.

that heating in the (outer) crust can produce surface temperatures which match the high magnetar surface temperatures; this is in agreement with the findings of Kaminker et al. (2006, 2009). On the other hand, even using a more realistic core heating prescription that includes magnetic field strength and temperature dependencies (as suggested by Dall’Osso et al. 2009), heating of the core by magnetic field decay produces T_s^∞ that are too low to explain the observed temperatures of magnetars. Only for extreme ($B_0 > 10^{16}$ G) and long-lived ($\tau_{\text{decay}} \gtrsim 10^3$ yr) magnetic fields and a magnetic, fully accreted light element envelope (which is unlikely due to diffusive nuclear burning in the hot surface layers; Chang & Bildsten 2004) could a surface temperature at the low end of magnetar temperatures ($T_s^\infty \sim 3 \times 10^6$ K) be produced. Therefore core heating alone cannot explain magnetar surface temperatures.

3.6 Onset of core neutron superfluidity with proton superconductivity

From Figs. 4 – 6, we see that the onset of core neutron superfluidity can be delayed from age a few $\times 100$ yr when the initial core field $B_0 \lesssim \text{a few} \times 10^{15}$ G to, e.g., $\approx 10^4$ yr when $B_0 = 5 \times 10^{15}$ G (and $\tau_{\text{decay}} = 10^4$ yr) or 3×10^4 yr when $B_0 = 8 \times 10^{16}$ G (and $\tau_{\text{decay}} = 10^3$ yr). This is based on our simple model of core heating, especially the assumption that field decay occurs on the timescale given by eq. (18). For the deep neutron triplet model (see Sec. 2.3), onset occurs earlier since the inner core cools faster and the maximum T_{cnt} is higher than in the shallow model (see Fig. 2).

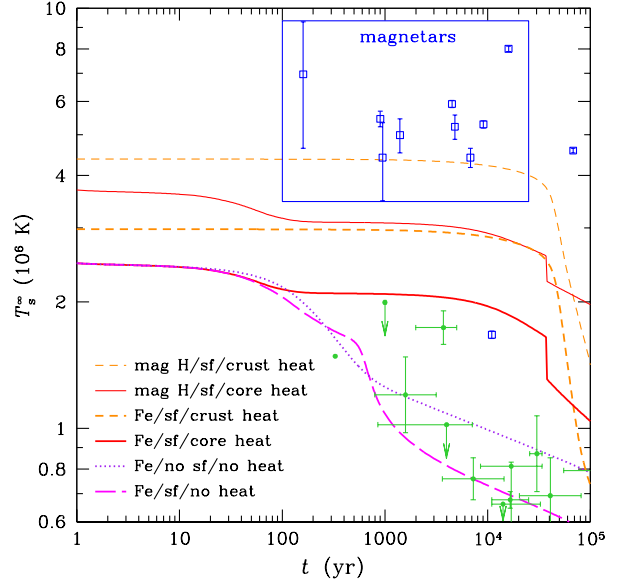


Figure 7. Redshifted surface temperature evolution for models with no superfluid (dotted line), superfluid and no heating (long-dashed line), superfluid and crust heating for heating timescale $\tau_h = 10^4$ yr (short-dashed lines), and superfluid and core heating for initial magnetic field $B_0 = 10^{16}$ G and field decay timescale $\tau_{\text{decay}} = 10^4$ yr (solid lines); the thin upper lines have fully accreted light-element envelopes (with a 10^{15} G radial surface magnetic field), while the thick lower lines have iron envelopes. Data points are magnetars and other neutron stars taken from the McGill SGR/AXP Online Catalog and those listed in Chevalier (2005); Yakovlev et al. (2008); Ho & Heinke (2009); Kaminker et al. (2009), respectively.

The decay timescale given by eq. (18) is the timescale for the solenoidal mode of ambipolar diffusion of normal (non-superconducting) protons (Goldreich & Reisenegger 1992; Thompson & Duncan 1996). At lower temperatures (later times), there is a transition of ambipolar diffusion from the solenoidal to the non-solenoidal mode. This latter mode is driven by departure from beta chemical equilibrium and has a timescale (Goldreich & Reisenegger 1992)

$$\tau^{\text{nsol}} \sim 240 \text{ yr } (\rho/\rho_{\text{nuc}})^{4/3} (B/10^{16} \text{ G})^{-2} (T/10^9 \text{ K})^{-6}, \quad (20)$$

and the transition occurs at temperature

$$T^{\text{tr}} = 7 \times 10^8 \text{ K } (\rho/\rho_{\text{nuc}})^{1/12}. \quad (21)$$

Since $T_{\text{cp}} \sim (2 - 3) \times 10^9$ K (Page et al. 2011; Shternin et al. 2011), proton superconductivity occurs very early. When protons are superconducting (and neutrons are normal), processes involving protons are suppressed (see Glampedakis et al. 2011, for more detailed calculation). In particular, the beta equilibrium reaction rate is reduced by a factor R_{pA} , which depends only on the ratio T/T_{cp} (Haensel et al. 2001), and the solenoidal and non-solenoidal ambipolar diffusion timescales are given by

$$\tau_{\text{sc}}^{\text{sol}} = (\tilde{R}_p B / H_{c1}) \tau^{\text{amb}} \quad (22)$$

$$\tau_{\text{sc}}^{\text{nsol}} = (B / H_{c1} R_{pA}) \tau^{\text{nsol}}, \quad (23)$$

respectively, where H_{c1} ($\approx 10^{15}$ G) is the first critical magnetic field, $\tilde{R}_p [= R_p + (m_e^*/m_e)(D_{\text{en}}/D_{\text{pn}})]$ is

the reduction factor modified to account for electron-neutron collisions, R_p is the reduction factor of proton-neutron collisions given in Baiko et al. (2001), and $D_{en} = 10^{14} \text{ s}^{-1} (\rho/\rho_{\text{nuc}})^{-2/3} (T/10^9 \text{ K})^2$ and $D_{pn} = 4.8 \times 10^{18} \text{ s}^{-1} (\rho/\rho_{\text{nuc}})^{-1/3} (T/10^9 \text{ K})^2$ are the inverse relaxation timescales for e - n and p - n collisions, respectively (Yakovlev & Shalybkov 1990). The transition temperature also increases, i.e.,

$$T_{\text{sc}}^{\text{tr}} = (R_{pA} \tilde{R}_p)^{-1/8} T^{\text{tr}}. \quad (24)$$

Thus the heating rate in the core due to magnetic field decay by ambipolar diffusion of normal or superfluid protons is given by eq. (17),⁷ where

$$\tau^{\text{amb}} \rightarrow \tau_{\text{sc}}^{\text{amb}} = \begin{cases} \tau^{\text{amb}} & \text{if } T > T_{\text{cp}} \\ \tau_{\text{sc}}^{\text{sol}} & \text{if } T_{\text{sc}}^{\text{tr}} < T < T_{\text{cp}} \\ \tau_{\text{sc}}^{\text{nsol}} & \text{if } T < T_{\text{sc}}^{\text{tr}} \end{cases} \quad (25)$$

and illustrated in Fig. 8 for typical parameter values. Note the removal of one power of B in $\tau_{\text{sc}}^{\text{amb}}$ at $T < T_{\text{cp}}$ and the strong increase in $\tau_{\text{sc}}^{\text{amb}}$ ($\propto R_{pA}^{-1} T^{-6}$) at low temperatures. Using this heating rate (that accounts for superconducting protons) in our cooling calculations, we find that there is *no delay* in the onset of core neutron superfluidity. Onset occurs at a few $\times 100$ yr, and the temperature profile/evolution is very similar to the case without core heating (see Figs. 4 and 5) for any field $\lesssim 10^{16}$ G (however, at the high field end, superconductivity is expected to be suppressed; Baym et al. 1969). This is because proton superconductivity greatly increases the timescale for field decay, which consequently reduces Q_h and renders core heating ineffective against cooling by strong neutrino emission.

4 DISCUSSION

We performed detailed calculations of neutron star cooling, including the effects of superfluidity and additional heating (due to magnetic field decay) in the crust and core. We find that magnetic field decay in the neutron star core cannot be the sole source powering the high observed surface temperature of magnetars in quiescence; the high temperatures require outer crust heating (Kaminker et al. 2006, 2009). Because of crust heating and effective thermal decoupling between the outer crust and core, the state of matter in the core cannot be deduced from these surface temperature measurements. By computing the evolution of the temperature profile $T(\rho)$, we determine the time when core neutrons first become superfluid, i.e., when $T < T_{\text{cnt}}(\rho)$. We find that heating by field decay in the core (with fields $\lesssim 10^{16}$ G) cannot balance neutrino cooling and thus cannot maintain relatively high core temperatures (c.f., Thompson & Duncan 1996; Dall’Osso et al. 2009). As a result, onset of superfluidity for neutrons in the core cannot be delayed, and neutron stars possess superfluid and superconducting cores after a few hundred years; this does not strongly depend on the nuclear EOS. Since core heating is not significant, the temperature profiles $T(\rho)$ and surface temperature evolution

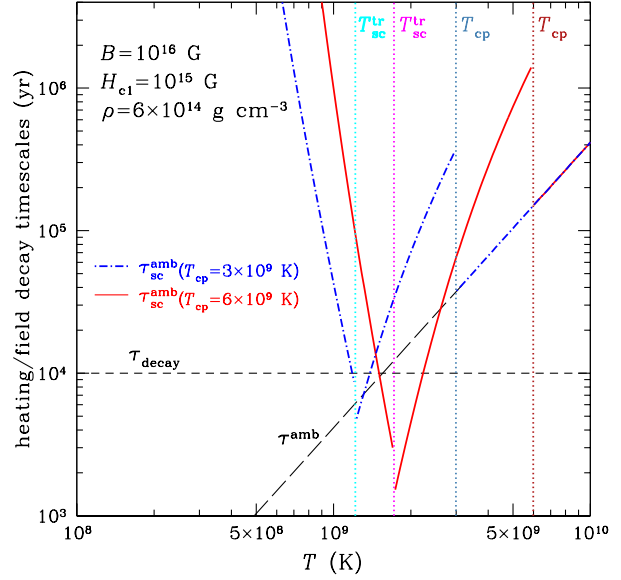


Figure 8. Core heating and field decay timescales used in this work as a function of temperature for typical parameter values. Long-dashed line is (solenoidal) ambipolar diffusion timescale τ^{amb} in normal matter [see eq. (18)], dot-dashed and solid lines are ambipolar diffusion timescales $\tau_{\text{sc}}^{\text{amb}}$ which account for proton superconductivity at $T_{\text{cp}} = 3 \times 10^9$ K and 6×10^9 K, respectively [see eq. (25)], and short-dashed line is the field decay timescale $\tau_{\text{decay}} [= 10^4 \text{ yr}]$; see eq. (19)]. Vertical dotted lines denote the critical temperatures for proton superconductivity T_{cp} and temperatures for transition between solenoidal and non-solenoidal modes of ambipolar diffusion $T_{\text{sc}}^{\text{tr}}$ [see eq. (24)].

$T_s^\infty(t)$ for magnetars are just those with crust heating (see Figs. 5 and 7, respectively), and crust heating does not affect the onset of core neutron superfluidity because of thermal decoupling between the outer crust and core.

Magnetar activity may be driven by field decay in the core (Thompson & Duncan 1995, 1996) or by processes in the crust (Thompson & Duncan 1993, 1995; Glampedakis et al. 2011; Price et al. 2012). Although the former may still be true, it must be accompanied by heating in the (outer) crust. On the other hand, field evolution in the crust easily couples to surface emission. Thus in order to understand the high surface temperature of magnetars, detailed studies should focus on magnetic field evolution and heating in the crust (see, e.g., Pons et al. 2009; Cooper & Kaplan 2010; Price et al. 2012). We note that several magnetars may have very similar X-ray luminosities (Durant & van Kerkwijk 2006); this could suggest that their crustal field strengths are similar and the field decay timescale is longer than the age of these sources.

Finally, the (normal versus superfluid) state of the core has important consequences for magnetic and rotational evolution of magnetars (Glampedakis & Andersson 2011), as well as their glitching behavior and possible stellar oscillations; studies of these effects may be effective probes of the neutron star core. We showed that the core can be treated as being in a superfluid and superconducting state after the neutron star is a few hundred years old.

⁷ The heating rate could be further corrected by using $Q_h \sim H_{c1} B / 4\pi \tau_{\text{sc}}^{\text{amb}}$ when the protons are superconducting. This would make core heating even less important at strong fields.

ACKNOWLEDGMENTS

WCGH thanks Dmitry Yakovlev for valuable comments on an early version of the manuscript. WCGH appreciates the use of the computer facilities at the Kavli Institute for Particle Astrophysics and Cosmology. WCGH and NA acknowledge support from the Science and Technology Facilities Council (STFC) in the UK. KG is supported by the Ramón y Cajal Programme of the Spanish Ministerio de Ciencia e Innovación.

REFERENCES

- Aguilera, D. N., Pons, J. A., & Miralles, J. A. 2008a, *A&A*, 486, 255
- Aguilera, D. N., Pons, J. A., & Miralles, J. A. 2008b, *ApJ*, 673, L167
- Aguilera, D. N., Cirigliano, V., Pons, J. A., Reddy, S., & Sharma, R. 2009, *Phys. Rev. Lett.*, 102, 091101
- Akmal, A., Pandharipande, V. R., & Ravenhall, D. G. 1998, *Phys. Rev. C*, 58, 1804
- Andersson, N., Comer, G., & Glampedakis, K. 2005, *Nucl. Phys. A*, 763, 212
- Arras, P., Cumming, A., & Thompson, C. 2004, *ApJ*, 608, L49
- Baiko, D. A., Haensel, P., & Yakovlev, D. G. 2001, *A&A*, 374, 151
- Baym, G., Pethick, C., & Pines, D. 1969, *Nature*, 224, 673
- Cassisi, S., Potekhin, A. Y., Pietrinferni, A., Catelan, M., & Salaris, M. 2007, *ApJ*, 661, 1094
- Chang, P. & Bildsten, L. 2004, *ApJ*, 616, L147
- Chang, P., Bildsten, L., & Arras, P. 2010, *ApJ*, 723, 719
- Chen, J. M. C., Clark, J. W., Davé, R. D., & Khodel, V. V. 1993, *Nucl. Phys. A*, 555, 59
- Chevalier, R. A. 2005, *ApJ*, 619, 839
- Chugunov, A. I. & Haensel, P. 2007, *MNRAS*, 381, 1143
- Colpi, M., Geppert, U., & Page, D. 2000, *ApJ*, 529, L29
- Cooper, R. L. & Kaplan, D. L. 2010, *ApJ*, 708, L80
- Dall’Osso, S., Shore, S. N., & Stella, L. 2009, *MNRAS*, 398, 1869
- Demorest, P. B., Pennucci, T., Ransom, S. M. Roberts, M. S. E., & Hessels, J. W. T. 2010, *Nature*, 467, 1081
- Durant, M. & van Kerkwijk, M. H. 2006, *ApJ*, 650, 1070
- Elgarøy, Ø., Engvik, L., Hjorth-Jensen, M., & Osnes, E. 1996, *Nucl. Phys. A*, 607, 425
- Flowers, E. & Itoh, N. 1979, *ApJ*, 230, 847
- Flowers, E. & Itoh, N. 1981, *ApJ*, 250, 750
- Geppert, U., Küker, M., & Page, D. 2004, *A&A*, 426, 267
- Glampedakis, K. & Andersson, N. 2011, *ApJ*, 740, L35
- Glampedakis, K., Andersson, N., & Lander, S. K. 2012, *MNRAS*, 420, 1263
- Glampedakis, K., Jones, D. I., & Samuelsson, L. 2011, *MNRAS*, 413, 2021
- Gnedin, O. Y., Yakovlev, D. G., & Potekhin, A. Y. 2001, *MNRAS*, 324, 725
- Goldreich, P. & Reisenegger, A. 1992, *ApJ*, 395, 250
- Gudmundsson, E. H., Pethick, C. J., & Epstein, R. I. 1982, *ApJ*, 259, L19
- Gusakov, M. E., Kaminker, A. D., Yakovlev, D. G., & Gnedin, O. Y. 2004, *A&A*, 423, 1063
- Gusakov, M. E., Kaminker, A. D., Yakovlev, D. G., Gnedin, O. Y. 2005, *MNRAS*, 363, 555
- Haensel, P., Levenfish, K. P., & Yakovlev, D. G. 2001, *A&A*, 372, 130
- Haensel, P., Potekhin, A. Y., & Yakovlev, D. G. 2007, *Neutron Stars 1. Equation of State and Structure*. Springer, New York
- Haensel, P., Urpin, V. A., & Yakovlev, D. G. 1990, *A&A*, 229, 133
- Heinke, C. O. & Ho, W. C. G. 2010, *ApJ*, 719, L167
- Heiselberg, H. & Hjorth-Jensen, M. 1999, *ApJ*, 525, L45
- Heyl, J. S. & Kulkarni, S. R. 1998, *ApJ*, 506, L61
- Ho, W. C. G. & Heinke, C. O. 2009, *Nature*, 462, 71
- Kaminker, A. D., Yakovlev, D. G., & Gnedin, O. Y. 2002, *A&A*, 383, 1076
- Kaminker, A. D., Yakovlev, D. G., Potekhin, A. Y., Shibazaki, N., Shternin, P. S., & Gnedin, O. Y. 2006, *MNRAS*, 371, 477
- Kaminker, A. D., Potekhin, A. Y., Yakovlev, D. G., & Chabrier, G. 2009, *MNRAS*, 395, 2257
- Lai, D. 2001, *Rev. Mod. Phys.*, 73, 629
- Lander, S. K., Andersson, N., & Glampedakis, K., 2012, *MNRAS*, 419, 732
- Lattimer, J. L. & Prakash, M. 2004, *Science*, 304, 536
- Lattimer, J. M., van Riper, K. A., Prakash, M., & Prakash, M. 1994, *ApJ*, 425, 802
- Levenfish, K. P. & Yakovlev, D. G. 1994a, *Astron. Rep.*, 38, 247
- Levenfish, K. P. & Yakovlev, D. G. 1994b, *Astron. Lett.*, 20, 43
- Lombardo, U. & Schulze, H.-J. 2001, in Blaschke, D. Glendenning, N. K., Sedrakian, A., eds, *LNP 578, Physics of Neutron Star Interiors*. Springer-Verlag, Berlin, p.30
- Mereghetti, S. 2008, *A&A Rev.*, 15, 225
- Negele, J. W. & Vautherin, D. 1973, *Nucl. Phys. A*, 207, 298
- Oyamatsu, K. 1993, *Nucl. Phys. A*, 561, 431
- Page, D., Geppert, U., & Weber, F. 2006, *Nucl. Phys. A*, 777, 497
- Page, D., Lattimer, J. M., Prakash, M., & Steiner, A. W. 2004, *ApJS*, 155, 623
- Page, D., Lattimer, J. M., Prakash, M., & Steiner, A. W. 2009, *ApJ*, 707, 1131
- Page, D., Prakash, M., Lattimer, J. M., & Steiner, A. W. 2011, *Phys. Rev. Lett.*, 106, 081101
- Passamonti, A. & Andersson, N. 2011, *MNRAS*, 413, 47
- Pons, J. A., Miralles, J. A., & Geppert, U. 2009, *A&A*, 496, 207
- Potekhin, A. Y. 1999, *A&A*, 351, 787
- Potekhin, A. Y. & Yakovlev, D. G. 2001, *A&A*, 374, 213
- Potekhin, A. Y., Chabrier, G., & Yakovlev, D. G. 1997, *A&A*, 323, 415
- Potekhin, A. Y., Baiko, D. A., Haensel, P., & Yakovlev, D. G. 1999, *A&A*, 346, 345
- Potekhin, A. Y., Yakovlev, D. G., Chabrier, G., & Gnedin, O. Y. 2003, *ApJ*, 594, 404
- Price, S., Link, B., Epstein, R. I., & Li, H. 2012, *MNRAS*, 420, 949
- Rea, N. et al. 2010, *Science*, 330, 944
- Rüster, S. B., Hempel, M. & Schaffner-Bielich, J. 2006, *Phys. Rev. C*, 73, 035804
- Sauls, J. A. 1989 in Ögelman, H., van den Heuvel, E. P. J., eds, *Timing Neutron Stars*. Kluwer Academic, p. 457

- Shapiro, S. L. & Teukolsky, S. A. 1983, *Black Holes, White Dwarfs, and Neutron Stars*. John Wiley & Sons, New York
- Shternin, P. S. & Yakovlev, D. G. 2007, *Phys. Rev. D*, 75, 103004
- Shternin, P. S., Yakovlev, D. G., Heinke, C. O., Ho, W. C. G. & Patnaude, D. J. 2011, *MNRAS*, 412, L108
- Thompson, C. & Duncan, R. C. 1993, *ApJ*, 408, 194
- Thompson, C. & Duncan, R. C. 1995, *MNRAS*, 275, 255
- Thompson, C. & Duncan, R. C. 1996, *ApJ*, 473, 322
- Thorne, K. S. 1977, *ApJ*, 212, 825
- Tsuruta, S. 1998, *Phys. Rep.*, 292, 1
- van Riper, K. A., 1991, *ApJS*, 75, 449
- Wambach, J., Ainsworth, T. L., & Pines, D. 1993, *Nucl. Phys. A*, 555, 128
- Woods, P. M. & Thompson, C. 2006, in Lewin, W. H. G., van der Klis, M., eds, *Compact Stellar X-ray Sources*. Cambridge University Press, Cambridge, p. 547
- Yakovlev, D. G. & Kaminker, A. D. 1994, in Chabrier, G., Schatzman, E., eds, *IAU Colloq. 147: Equation of State in Astrophysics*. Cambridge University Press, Cambridge, p. 214
- Yakovlev, D. G. & Pethick, C. J. 2004, *ARA&A*, 42, 169
- Yakovlev, D. G. & Shalybkov, D. A. 1990, *Sov. Astron. Lett.*, 16, 86
- Yakovlev, D. G., Kaminker, A. D., & Levenfish, K. P. 1999a, *A&A*, 343, 650
- Yakovlev, D. G., Levenfish, K. P., & Shibano, Yu. A. 1999b, *Phys.-Uspekhi*, 42, 737
- Yakovlev, D. G., Gnedin, O. Y., Kaminker, A. D., & Potekhin, A. Y. 2008, in Bassa, C., Wang, Z., Cumming, A., Kaspi, V., eds, *AIP Conf. Proc. Vol. 983, 40 Years of Pulsars*. American Inst. Phys., Melville, NY, p. 379
- Yakovlev, D. G., Ho, W. C. G., Shternin, P. S., Heinke, C. O., & Potekhin, A. Y. 2011, *MNRAS*, 411, 1977
- Yakovlev, D. G., Kaminker, A. D., Gnedin, O. Y., & Haensel, P. 2001, *Phys. Rep.*, 354, 1